INSTITUTE OF PHYSICS PUBLISHING and INTERNATIONAL ATOMIC ENERGY AGENCY NUCLEAR FUSION

Nucl. Fusion **43** (2003) 1384–1395 PII: S0029-5515(03)70264-6

Transport studies with the ECH system on FTU tokamak

S. Cirant[1], G. Bracco[2], A. Bruschi[1], P. Buratti[2], F. De Luca[3], B. Esposito[2], F. Gandini[1], E. Giovannozzi[2], G. Granucci[1], A. Jacchia[1], E. Lazzaro[1], E. Minardi[1], S. Nowak[1], G. Ramponi[1], C. Sozzi[1], O. Tudisco[2] and FTU Team and ECRH Group[1]

[1] EURATOM Association, IFP CNR Milano, Italy
[2] EURATOM Association, ENEA Frascati, Italy
[3] I.N.F.M. and Dipartimento di Fisica, Università degli Studi di Milano via Celoria, 16 20133 Milano, Italy

E-mail: cirant@ifp.cnr.it

Received 9 December 2002, accepted for publication 8 October 2003
Published 3 November 2003
Online at stacks.iop.org/NF/43/1384

Abstract

Experiments performed on the FTU tokamak, aimed at validation of physics-based transport models, which yield the electron temperature profile stiffness by using electron cyclotron resonance heating (ECRH), and at the implementation of ECRH-based techniques for plasma real-time control, are presented. ECRH is used to probe transport features, both in the steady state and in response to time-varied heating. The experiments clearly show stiffness in the electron temperature profile response to localized ECRH. The low gradient plasma region near the axis is characterized by low stiffness, in the sense that the temperature gradient can change with increasing heat flux, and low electron thermal diffusivity. Strong stiffness (in the sense that the temperature gradient length $1/L_T = -\nabla T/T$ does not change significantly even with significantly different heating profiles and intensity) and high diffusivity are found in the confinement region ($0.15 < r/a < 0.5$). Particular attention is given to the experimental investigation of the transition layer between low and high diffusivity (and low and high stiffness) regions, which is located at the EC deposition radius r_{dep} when powerful ECRH is applied. A transition layer, identified by heat waves launched by modulated ECH, is found also in plasmas with dominant Ohmic heating, showing that it is a local plasma feature, and not merely a consequence of a step-wise increase in the conducted heat flux at r_{dep}. All observations fit well with a critical temperature gradient length modelling of local electron heat transport.

The measurement of the rate of change of stored electron energy when ECRH is switched on (or off) is the basis of a technique for real-time and automatic detection of the absorption layer. Repetitive short pulses are used to increase the signal to noise ratio, with a very low duty cycle, so as not to waste ECRH power during the detection procedure.

PACS numbers: 52.25.Fi, 52.50.sw

1. Introduction

Electron cyclotron resonance heating (ECRH) experiments have an advantage in that there is potential for localized heating or current drive, which can be used in the study and in the active control of basic physical processes governing plasma stability and energy transport. One of the most successful uses of ECRH in tokamaks is in MHD activity control, and in particular tearing mode (TM) [1, 2], neoclassical TMs (NTMs) [3] and sawteeth mitigation/stabilization [4–6], to the point that closed loop systems for automatic control/suppression of MHD activity in fusion devices are being implemented [7, 8]. More and more insight into electron transport is being gained by studying the plasma response to precisely localized heat deposition, both in steady state and transient conditions. The FTU tokamak has been active in all these fields with experiments performed with an r.f. system at 140 GHz, 2 MW, aiming both at basic physics research and at technological developments. This paper focuses on recent achievements in electron transport studies and in the closely related, although more technological, application of automatic control of the deposition radius of EC waves.

Concerning energy confinement, the use of ECRH in FTU has clearly shown [9, 10], contemporarily to other tokamaks [11, 12], the property of electron temperature profile stiffness. The experimental observation of profile stiffness with ECRH

is that an accumulation of the heating power density P_{heating} at the EC waves deposition radius r_{dep} does not cause a change in the T_e profile curvature $\nabla^2 T_e$, which is expected when the heat continuity condition, $\nabla \cdot (-n_e \chi_e \nabla T_e) = P_{\text{heating}}$ in the steady state is considered. Profile stiffness implies that the electron heat diffusivity χ_e must adjust itself during ECRH to keep the gradient ∇T_e flat, in a way that is incompatible with a smooth dependence of χ_e on local plasma parameters.

The experimental observation of profile stiffness is being interpreted both on the basis of profile consistency [13, 14], and of an electron heat transport driven by turbulence, with a threshold on the temperature gradient length $L_T = -T_e/\nabla T_e$ [15–17]. Although in both approaches the profile shape shows invariant features, it is worth noting that in the first case concerning consistency the thermal diffusivity χ_e is a derived quantity, which follows from global constraints that first determine the various profile shapes. In the second case concerning turbulence driven transport, χ_e is the measure of a local transport characteristic that relates the local temperature gradient with a given heat flux. The experiments described in this paper were performed with the objective of validating electron heat transport models, of testing in particular the stiffness of the electron temperature profile, and establishing similarities with other experiments in the same field [16]. Modulated ECH was also used for investigation of heat wave propagation and transient heat transport properties.

ECRH is mature for real-time applications of profile shaping, with precisely controlled localized deposition. This practice will be essential for steady maintenance of optimum conditions in fusion devices, but it will also be useful for more effective experiments in present day long pulse machines. The same localization of EC wave absorption, being linked to the laboratory frame where the magnets are firmly fixed, demands some flexibility in the launching system to precisely adapt itself to plasma evolutions in the laboratory frame. Preliminary to real-time control is the real-time recognition of the EC deposition radius, which is discussed in the last part of this work.

2. The EC heating system

ECRH is applied to FTU plasmas by launching up to 4 beams at a frequency of $f_{\text{ECH}} = 140\,\text{GHz}$, aiming at absorption at the fundamental EC resonance. Each beam is poloidally and toroidally steerable, and carries up to $P_{\text{ECH}} = 400\,\text{kW}$ of r.f. power. The EC beams are launched from the low field side of the tokamak, polarized for optimum coupling to the ordinary mode in the plasma [18]. Gyrotrons are powered in pairs, each couple sharing one of the two series tetrode regulating units (70 kV, 25 A) of the HV power supply. Each regulator has its own reference signal, so that two completely independent timings can be programmed for the gyrotron pairs.

The targets are quasi-circular plasmas in the L-mode confinement regime. The typical plasma current in the experiments described in this work is $I_p \approx 400\,\text{kA}$, $q_a \approx 6$, with an Ohmic input power of $P_{\text{OH}} \approx 500\,\text{kW}$, dropping to $P_{\text{OH}} \approx 250\,\text{kW}$ during EC heating. Since the cut-off density for the O-mode at the fundamental EC frequency is $n_{e,c.o.} = 2.4 \times 10^{20}\,\text{m}^{-3}$, target plasmas with a peak value $n_{e,0} \approx 1 \times 10^{20}\,\text{m}^{-3}$ are routinely used during ECRH without the appearance of strong refraction effects. In spite of the relatively high density with respect to most other ECRH experiments, e–i coupling still allows for less than 30% of the electron power input to be transferred to the ions, and $T_e/T_i > 2$ in all the experiments described in this paper. Even this small amount of ion thermal coupling is enough to create conditions in which during ECRH, and particularly during off-axis ECRH, the local electron power balance at steady state, including radiation losses, is negative everywhere but at the very localized EC deposition layer. This emphasizes the fact that the electron temperature profile shape is completely dominated by heat transport processes inside the plasma column, and stresses the potential of ECRH in studying the physics of electron energy transport.

3. Local and global aspects of profile stiffness

Unique features characterize profile stiffness: the saturation of the gradient length $L_T = -T_e/\nabla T_e$ and, in case of heating strongly localized at r_{dep}, a step-wise radial dependence of the effective electron thermal diffusivity $\chi_{e,PB} = -\Phi_{\text{heat}}/n_e \nabla T_e$ at r_{dep}. When ECRH is used as the main additional heating system in the FTU tokamak the normalized inverse gradient length R/L_T of the steady profile is bounded in a narrow band around $R/L_{T,c} \approx 10$, in spite of the wide range of heating power ($P_{\text{OH}} = 200$–$1000\,\text{kW}$; $P_{\text{ECRH}} = 0$–$750\,\text{kW}$) and power density applied. Saturation occurs in a finite radial layer with inner and outer margins varying with the specific discharge conditions (high–low electron density; high–low P_{ECRH}; at flat-top or during current ramp-up, etc), but always in the region $0.15 < r/a < 0.6$.

An example of this behaviour is shown in figure 1, in which a five-times increase in the heat flux in the same shot does not change ∇T_e as much. L_T dependence on the radius is similar in all cases: after an increase in the core up to $r/a \approx 0.2$, it flattens around $L_T = 9.5 \pm 1.5$, up to $r/a \approx 0.4$. While on the outer side of the EC absorption layer the heat flux strongly increases

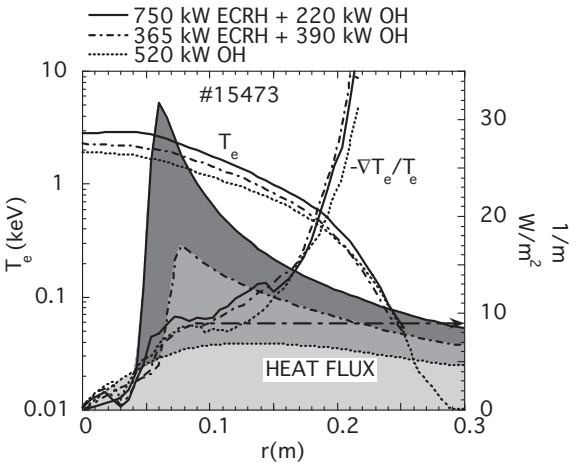

Figure 1. Electron temperature, gradient length and heat flux versus radius for different levels of ECRH intensity. The electron temperature gradient length does not increase with stronger heating. Note that the major radius being $R \approx 0.98\,\text{m}$, $1/L_T$ can be directly used for normalized comparisons.

with ECRH, on the inner side it drops significantly because of loss of Ohmic heating in the core due to T_e increase. Since ∇T_e does not change so much across r_{dep}, and particularly in the outside region, it follows that $\chi_{e,PB}$ has a step-wise radial dependence at the deposition radius. This response is clearly shown in figure 2, and it represents a distinctive feature of profile stiffness in tokamaks.

This step in χ_e at r_{dep} is also detected by heat wave propagation experiments [12]: a first gyrotron is used in the CW mode to create a step in $\chi_{e,HP}$ and a second one is modulated to launch a heat wave for probing the effects on diffusivity caused by the first. A typical result from FTU is shown in figure 3, in which the amplitude of a heat wave propagating across the absorption layer of a second EC beam, kept on continuously, is described. The wave is generated by modulating the power

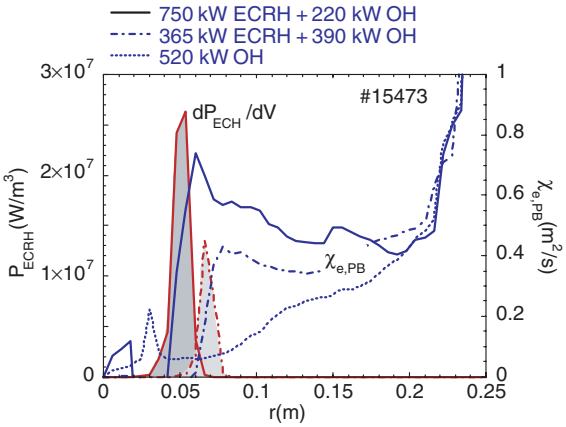

Figure 2. In order to maintain the temperature gradient length L_T constant also during ECRH, and smooth across the absorption layer, the electron thermal diffusivity χ_e develops a step at a deposition radius r_{dep}, larger with stronger heating.

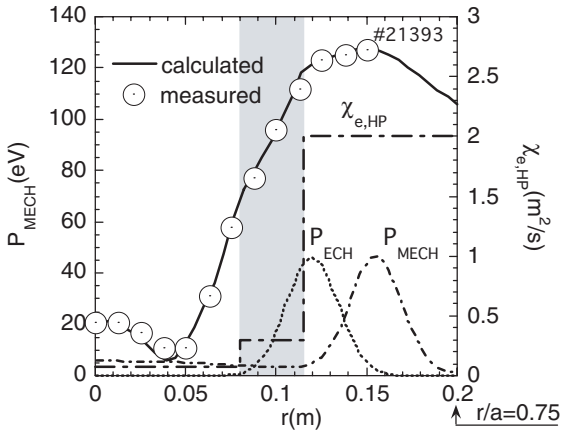

Figure 3. The inward heat wave generated by the absorption (power deposition profile peaked at $r = 0.155$ m in the figure) of a modulated EC beam reveals the down-step of the electron thermal diffusivity $\chi_{e,HP}$ at the absorption radius of a second EC beam (absorption peaked at $r = 0.12$ m) continuously on. The measured amplitude damping rate is strongly enhanced after passing through the CW beam absorption layer. Incomplete single pass absorption produces stray heating over the whole plasma column, as shown in the figure. This makes difficult and ambiguous the analysis of the phase distribution, not shown in the figure.

in an EC beam absorbed externally to the CW one. The abrupt increase of the amplitude damping rate, given by amplitude decay per unit length, of the inward wave starting at $r \approx 0.08$–0.11 m ($r/a \approx 0.3$–0.4) is a clear sign of a drop in diffusivity occurring in that region, and extending up to the plasma centre.

The occurrence of a drop in $\chi_{e,HP}$ to explain the damping rate discontinuity can be justified qualitatively by using a simple model for heat wave propagation in layered media [17], in which $\chi_{e,HP}$ has a step-wise dependence on the radius. The oscillating temperature distribution is obtained by solving the diffusion equation for a periodic perturbation:

$$i\omega T_\omega(r) - \frac{1}{rn(r)}\frac{d}{dr}\left[rn(r)\chi_{HP}(r)\frac{dT_\omega(r)}{dr}\right] = \frac{P_\omega(r)}{1.5\,kn(r)},$$

where the source term P_ω has a Gaussian shape with centre and width given by ray-tracing calculations. Although the assumption of constant $\chi_{e,HP}$ everywhere but at transition might be an over-simplification, the model is very useful in showing that the amplitude of the heat wave at the centre is very sensitive to the electron thermal diffusivity, and that a step is indeed needed to interpret the results. Without a corresponding step in the local heat diffusivity, T_e oscillations could not be damped so strongly inside r_{dep} of the CW beam, and so weakly on the outside. In many cases the change in damping rate is not immediately visible from the raw experimental data, and the model is essential to show that even a small step in $\chi_{e,HP}$ gives a much better description of the data than a uniform heat diffusivity, $\chi_{e,HP}$, distribution. Last but not the least, the model provides an estimate of the $\chi_{e,HP}$ value in both regions, which can be compared with the corresponding $\chi_{e,PB}$.

The step-wise behaviour of $\chi_{e,PB}$ across r_{dep} cannot be explained convincingly with a dependence of $\chi_{e,PB}$ on T_e alone, because of the smooth behaviour of the electron temperature across the absorption radius. In contrast, an empirical model quite successful in describing both steady state and transient response to ECRH [16] is based on heat diffusivity strongly dependent on ∇T_e, with a threshold on L_T, given by

$$\chi_e = \chi_0 + \lambda T_e^\alpha \left(\frac{-\nabla T_e}{T_e} - \kappa\right)^\beta H\left(\frac{-\nabla T_e}{T_e} - \kappa\right). \qquad (1)$$

Here, H, is the Heaviside function of argument $(1/L_T - \kappa)$, describing the threshold-dependent behaviour of χ_e. The difference in diffusivity on the opposite sides with respect to r_{dep} is associated with the intrinsic jump in the heat flux and in the associated thermal gradients. A similar relation has been successfully used to model FTU steady state discharges [15].

An additional feature supporting the observation of profile stiffness, and of the difference between plasma core and outer regions, is found by looking directly at the capability of the temperature profile itself to adapt locally to the power deposition profile according to the heat continuity condition (at constant χ_e). Because of the good localization of EC wave absorption, and consequent heating power density, which can be an order of magnitude larger than the Ohmic contribution, ECRH is ideal for carrying out tests on profile stiffness. The resistance of the steady state temperature profile to bend with localized ECRH can be quantified by a 'stiffness index' ξ [10], defined as the ratio $\Delta(\nabla^2 T)/\Delta P_{heating}$ between the relative change in profile curvature at the absorption layer, and the relative change in total power in the same volume.

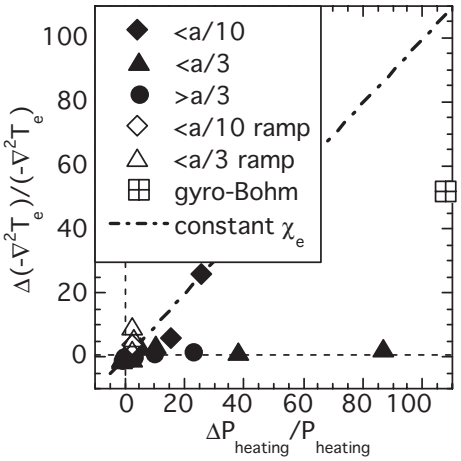

Figure 4. The figure suggests an objective definition of stiffness, which is seen as the reluctance of the temperature profile to adjust its curvature to localized heating. The relative change given by the ratio $\Delta(\nabla^2 T)/\nabla^2 T$, in the profile curvature in the absorption layer, and the corresponding change in the local heating intensity $\Delta P/P$, are considered. For reference, the line expected in the case of a plasma with constant $\chi_{e,PB}$ is also shown. A point below the reference line characterizes stiff profiles, the distance being larger with stronger stiffness.

The experimental estimate of $\Delta(\nabla^2 T)$ is derived directly from the measured T_e profile, the other one ($\Delta P_{heating}$) being essentially equal to P_{ECRH}. Since the ECRH power dominates over Ohmic heating in the absorption layer, the correction for a change in local Ohmic heating is small.

For a non-stiff profile the local curvature follows the increase in heating power, and therefore $\xi \approx 1$. Instead, stiffness implies that $\xi < 1$, since the gradients do not change as the heat fluxes do. For a completely rigid profile ξ would be zero.

Figure 4 shows that profile stiffness is maximum off-axis, and stronger with increasing local heating power density. In contrast, profiles can be non-stiff in the central region, provided that localized additional heating is not excessively strong, and there is always a non-stiff response on switching off the additional ECRH power (relative change $\Delta P/P = -P_{ECRH}/(P_{ECRH} + P_{OH}) \approx -1$). All these features are consistent with the critical gradient length model predictions.

The basic assumption of this empirical model is, therefore, that the heat conduction is strongly enhanced if the heat flux drives the gradient length below a critical threshold. This leads to a self-organization of the plasma column which creates a central region characterized by a large gradient length, low diffusivity and low stiffness, and an outer region characterized by high diffusivity, strong stiffness and saturated gradient length.

The transition layer between the two volumes, located where the heat flux and the local diffusivity bring the gradient length close to a critical value, is therefore a very peculiar region in the plasma. It is very sensitive to background transport, heat flux, and critical value of the gradient length, and strongly non-linear effects are expected to occur there. Its own existence gives a robust support to the whole critical gradient length based transport model, so that it is worthy of accurate experimental investigation.

The experimental investigation of the properties of the transition layer in thermal diffusivity, if any, is therefore crucial in the validation of the whole concept of transport based on critical gradient length. The comparison between model predictions and experimental data was, in fact, the main goal of the experiments described here.

Great care was exercised so as to distinguish a gradient driven transition from similar effects related to MHD and sawteeth, possibly occurring at, or close to, the $q = 1$ surface.

To this end ECRH was used to suppress sawteeth and to remove the $q = 1$ surface, or at least to move the resonant surface as close as possible to the plasma axis.

4. Transition layer

As already mentioned, the transition layer dividing the central low-diffusivity core from the external region, characterized by enhanced transport, coincides with r_{dep} when strong and localized ECRH is applied. However, equation (1), and the model itself, suggest that, independently of ECRH, the step in χ_e should be found in Ohmic plasmas as well. This follows from the fact that the electron diffusivity $\chi_{e,PB}$ is so low at the centre that the Ohmic heating flux alone would be sufficient to force $1/L_T$ towards κ somewhere in this well-confined plasma region.

The evidence that the step in $\chi_{e,HP}$ does not necessarily coincide with r_{dep}, but rather with the L_T saturation point, was preliminarily observed on the FTU tokamak by modulating ECH during current ramp-up [17], and it has been confirmed with the series of experiments at the current flat-top described in this paper.

ECRH is used in these experiments primarily to launch the heat wave, which probes the plasma column in search of the transition region and of the step in $\chi_{e,HP}$. The absorption of the EC beam is kept, therefore, as far as possible off-axis, in order to keep to a minimum level the effect of the average ECRH power on the Ohmic plasma in the core. Furthermore, inward propagation takes full advantage of the fact that the central amplitude of a heat wave originating off-axis is very sensitive to confinement features in the core.

Data analysis is aimed, therefore, mostly at the recognition of a discontinuity in the radial distribution of both the phase velocity and the amplitude damping rate of the inward heat wave, which is characteristic of the discontinuity in $\chi_{e,HP}$. The analysis is supported by the use of the simple model for $\chi_{e,HP}$ previously described, in which the thermal diffusivity is assumed to be constant in time, but with a step-wise radial dependence. The two levels of $\chi_{e,HP}$, and the position of the discontinuity, are free parameters to be adjusted for obtaining a best fit of the experimental data.

Although in most cases the discontinuity is directly evident in the raw data set, the comparison with the model helps in identifying the transition and provides an estimate of $\chi_{e,HP}$ in the two regions. In addition, backing the data with model calculations provides information on the sensitivity of the result to experimental errors.

Off-axis absorption is essential for sawtooth control, which is important at least for two reasons: sawteeth suppression allows a more accurate heat wave analysis in the central region; as mentioned earlier, we have to separate

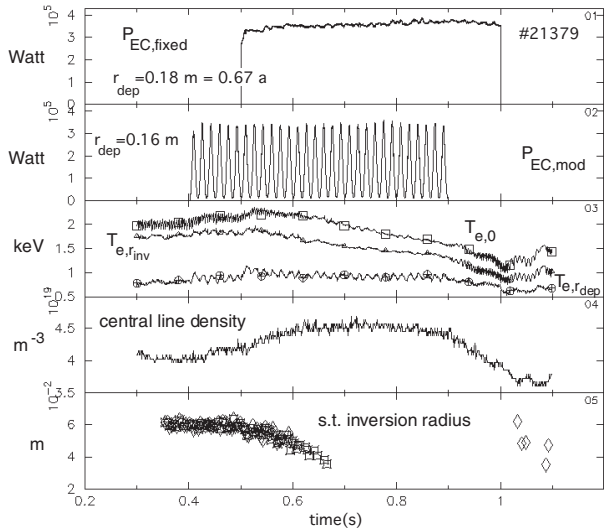

Figure 5. In order to limit as much as possible the impact of sawteeth on the analysis of the heat wave propagation towards the plasma centre, a second gyrotron at constant power can be used, absorbed at a larger radius to avoid interference with the inward wave. Top to bottom: CW ECRH power; modulated ECRH power; ECE electron temperature at centre, at the inversion radius and at the absorption radius; central line density; sawteeth inversion radius. As shown in the figure, a drawback of sawteeth stabilization is impurity (and electron density) accumulation in the core, with a drop in central temperature because of increased losses and density build-up.

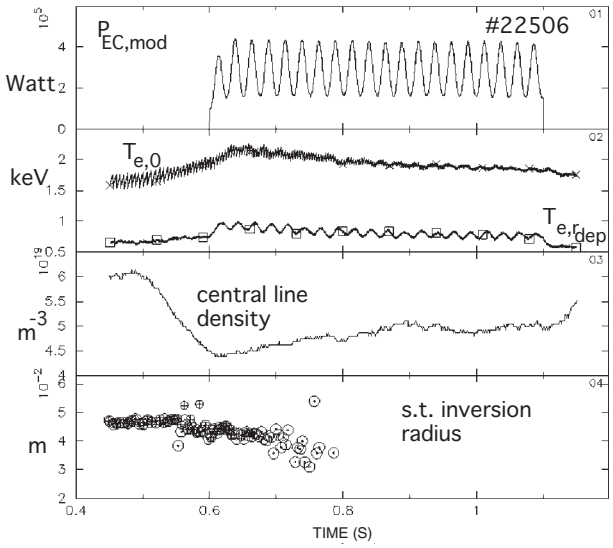

Figure 6. In case only one gyrotron has to be used for off-axis launch of an inward heat wave, sawteeth control can still be attempted by increasing the average value of the EC heating power at the expense of the modulation depth. Top to bottom: modulated ECRH power; ECE electron temperature at centre and at the absorption radius; central line density; sawteeth inversion radius. Heat wave propagation can be analysed in different time windows: during the sawteeth suppression phase, and after stabilization has taken place.

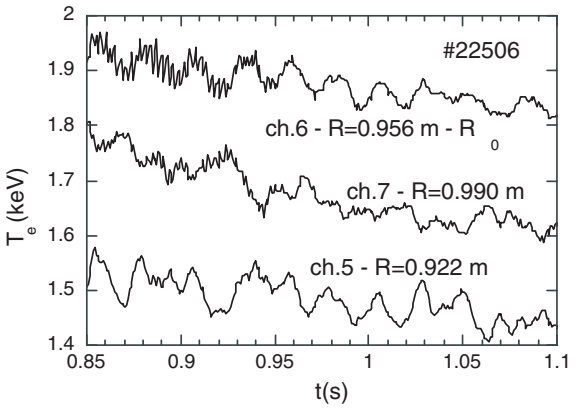

Figure 7. ECE electron temperature from the three channels closest to the axis, showing with more detail than in figure 6 sawteeth stabilization occurring at $t \approx 0.95$ s.

gradient driven effects from MHD effects. In some cases (e.g. shot #22506) the average ECRH power from one modulated gyrotron (400 kW peak-to-peak, 200 kW average) is sufficient to almost suppress sawteeth. In others (e.g. shot #21379), a second gyrotron is used CW, and with the power absorbed even more off-axis (figure 5) in order not to interfere with the inward heat wave propagation. Off-axis heating is achieved either by beam steering, or by $B_{\rm tor}$ adjustments, this last method being preferred since it avoids stray heating at the centre even in the case of incomplete single pass absorption of EC waves at resonance.

Heat wave propagation is observed on FTU at 12 values of the major radius by using a multi-channel ECE polychromator, tuned to 12 positions from $r_{\rm dep}$ up to the centre (the outward heat wave is ignored in these experiments).

The main result is that, in all the experiments, a sharp drop in $\chi_{\rm e,HP}$ was detected somewhere by the inward heat wave, in a position clearly separated from the EC absorption radius and from $q = 1$ related surfaces. Two representative discharges are described in the following, the first (shot #22506) at $I_{\rm p} = 300$ kA, $q_0 < 1$, with sawteeth in the Ohmic phase, which are suppressed by ECRH, and the second one (shot #22507) at $I_{\rm p} = 250$ kA, $q_{\rm a} = 8$, $q_0 \geqslant 1$, without sawteeth. It has to be noted that the q-profile is only estimated in FTU, since no direct measurement of the current density profile was available at the time the experiments were performed. However, in the case of a long, steady and quiescent flat-top, as was the case in these two example shots, power balance and equilibrium reconstruction are reliable. We could not obtain an acceptable power balance by fitting the experimental observables ($V_{\rm loop}$, $P_{\rm rad}$, $I_{\rm p}$) with q-profiles much different from those estimated.

In both cases, the electron line density on-axis is $n_{\rm e} = 0.6 \times 10^{20}\,{\rm m}^{-3}$, with marginal e–i coupling. The toroidal field on-axis is $B_{\rm tor} = 6$ Tesla, which sets the resonance layer at $r/a = 0.55$. The typical EC power modulation depth is $P_{\rm MECH} = 200$ kW peak-to-peak, on top of an average power of $P_{\rm ECH} = 300$ kW.

Shot #22506 (figure 6) is representative of the experiments performed on FTU to study the transition layer, in which one single gyrotron is used both to launch an inward heat wave and to stabilize sawteeth by an appropriate choice of the average power and modulation depth. Sawteeth stabilization is achieved with a time delay consistent with the current diffusion time from the absorption radius to the inversion radius [10]. Therefore, in the first time window (0.6–0.7 s) sawteeth are still active, although the inversion radius is progressively shrinking, while in the second one regular sawteeth activity disappears. Figure 7 shows that from $t \approx 0.95$ s onwards only sporadic,

low-amplitude reconnections possibly survive. Because of the finite spatial resolution of the ECE polychromator, one cannot exclude that sawteeth are still active very close to the axis, but in this case the whole inversion diameter should be less than the distance between channels 6 and 7, which is 3.5 cm in this case ($\delta r_{\rm ch}/2 \approx 1.75\,{\rm cm} = 0.06a$). As usual with sawteeth stabilization in the FTU tokamak [10], the central average temperature is slightly reduced by density peaking and by reduction of core heating caused by impurity accumulation and increased radiation losses. For a more comprehensive description of the MHD features of the discharge, the evolution of the $q = 1$ resonant surface position should be estimated, to complete the experimental evidence of an inversion radius shrinking from $r_{\rm inv} = 4.8\,{\rm cm}$ to less than 1.8 cm during sawteeth stabilization. In fact, sawtooth stabilization does not necessarily mean removal of the $q = 1$ surface [6, 19]. As already mentioned, the q-profile is estimated by equilibrium reconstruction, conditioned by power balance analysis. The results of the analysis are summarized in figures 8(a) and (b), showing, respectively, the time evolution of q-central and of the $q = 1$ radius. The change in q-central matches well the evolution in sawteeth amplitude (sawteeth are first enhanced by ECRH while q-central decreases; sawteeth are progressively stabilized while q-central increases towards unity). The estimated change in $r_{q=1}$ follows the experimentally measured decrease in $r_{\rm inv}$. The main conclusion concerning the (1, 1) mode dynamics in shot #22506 is that $r_{q=1}$ and $r_{\rm inv}$ are more than halved during ECRH, if not becoming zero.

Concerning electron transport, figures 9 and 10 show, respectively, the wave amplitude and phase in two time slots in the discharge, at the beginning and the end of the ECRH pulse. Since ECH modulation frequency and sawteeth repetition rate are quite different in this case, the two contributions to the overall oscillating temperature can be separated.

The experimental data can be described well by a stepped-$\chi_{\rm e,HP}$ diffusive model, which shows that the wave damping rate in the central region is always stronger than that in external regions. Although a strict comparison between data and model would suggest the occurrence of a double-step in the diffusivity drop for a best fit of the experiment, the main information provided by heat wave propagation is that a drop in $\chi_{\rm e,HP}$ exists, and that it must occur in a narrow layer at $r \approx 0.07$–0.1 m. A discontinuous profile of $\chi_{\rm e,HP}$ is, therefore, necessary to explain the experimental results.

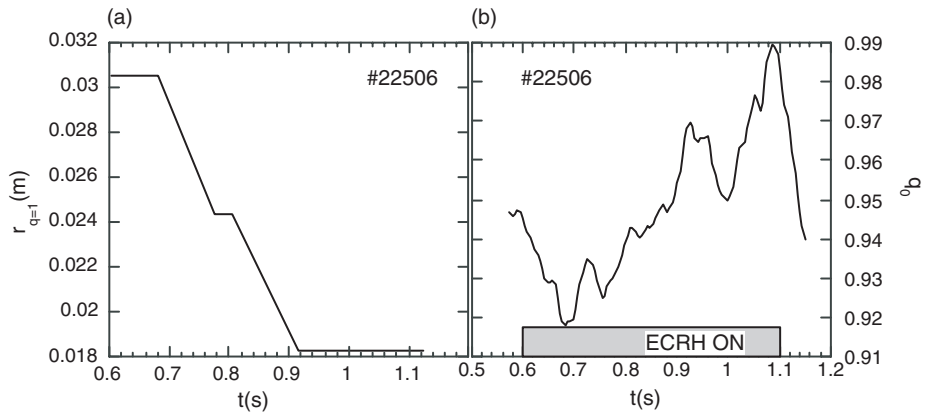

Figure 8. (a) shows the evolution in time of the $q = 1$ radius, (b) the central q is shown versus time. The q-profile is estimated by equilibrium reconstruction, conditioned by power balance analysis.

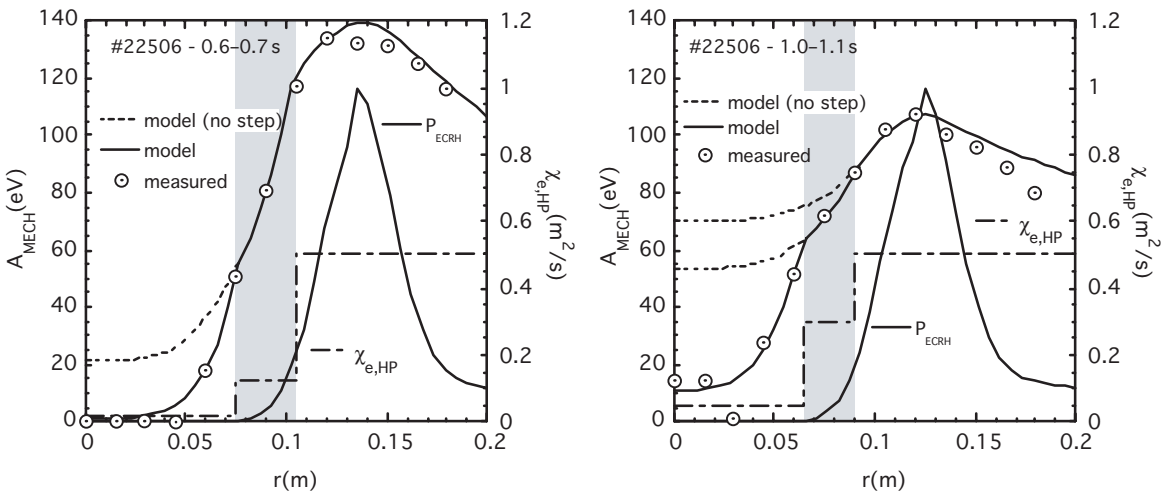

Figure 9. Amplitude distribution of the heat wave in the first time window (left) in shot #22506 shown in figure 6, still sawtoothing, and in the second time window, when sawteeth are suppressed. In both cases the wave detects a step-down in $\chi_{\rm e,HP}$, at approximately the same position (0.07–0.1 m), in spite of the likely change of the q-profile during sawteeth stabilization.

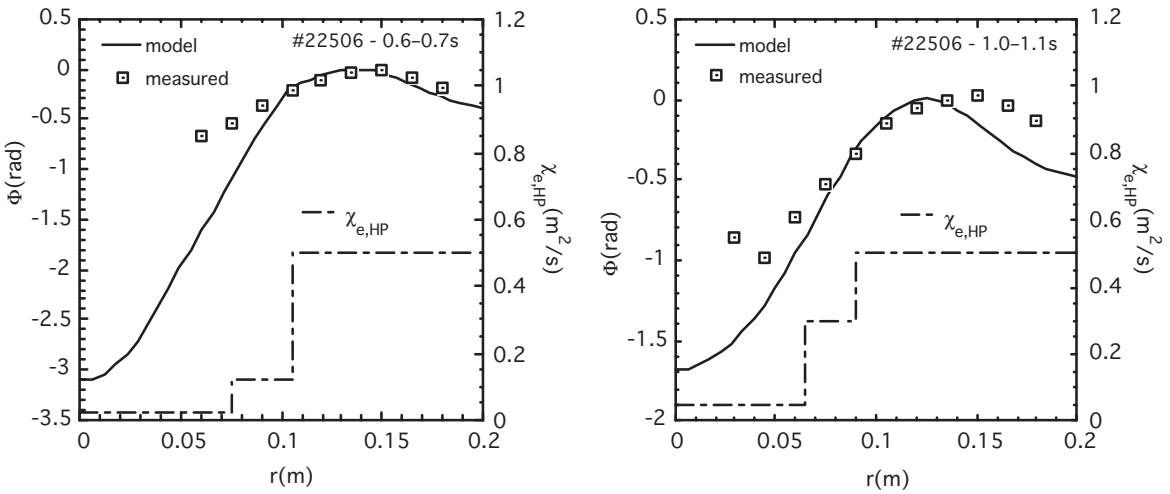

Figure 10. The phase distribution is also compatible with the step-down in $\chi_{e,HP}$, although in the first time window (at left) sawteeth might still affect the phase measurement. In both cases stray radiation (<5%) not completely absorbed at first pass contributes to the phase in the central region. Delocalized absorption taking place from the resonant radius up to the edge might cause direct peripheral heating at zero phase shift.

In all cases, if diffusivity were uniform down to the plasma axis, one should find much larger central oscillations than actually observed (in fact, in many cases the heat wave simply disappears at the centre).

The presence of a discontinuity in $\chi_{e,HP}$ is also consistent with phase measurements, although the observed discontinuity in the phase velocity appears to be less evident than the change in the amplitude damping rate. Factors affecting the phase measurements are related either to MHD (sawteeth, or a remaining $m = 1$ oscillation) or to stray EC absorption at radii external to the resonance. In both cases the effect would be to mask the phase change due to the pure heat wave propagation.

Figure 9 shows that the step in electron thermal diffusivity, clearly seen by heat waves propagating towards the centre, does not move as much as r_{inv}, or $r_{q=1}$, does during sawteeth stabilization. The layer is positioned around 7.5–10 cm during sawteeth, and around 6.5–9 cm without sawteeth. The change in the radial position of the transition layer is much smaller than the one of $r_{q=1}$ or r_{inv} which shrinks from 5–6 cm to less than 1.75 cm. These arguments support that, in this case at least, $r_{q=1} \neq r_{step}$.

In order to distinguish between $q = 1$ driven, and $\nabla T_{e,crit}$ dependent steps in electron transport, it would be clearly preferable to perform experiments in the absence of a $q = 1$ resonant surface. To do that, a low-current experiment was performed, with $q_a \approx 11$, $q_0 \geqslant 1$. As shown in figure 11, discharge #22507 is MHD stable, with a peaked T_e profile which adapts itself to the density and central Ohmic heating evolution. As usual in FTU, the density increases during ECRH mostly because of recycling modifications and density build-up starting at the edge, and the temperature drops according to the density increase. The central line density $n_{e,0} \approx 0.25 \times 10^{20}$ is relatively low in this discharge in order to prevent sawteeth appearance as much as possible. Low-density operation helps in the development of sawtooth free conditions during the current build up, which can also be maintained at current flat-top. EC waves are absorbed off-axis, further preventing sawtooth appearance during heat

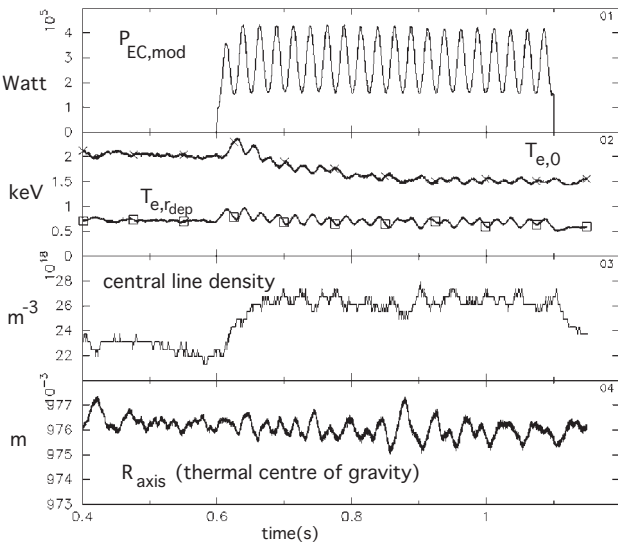

Figure 11. In order to avoid any possible effect of sawteeth on the heat wave propagation, a low current, high q ($q_a = 11$) discharge is used as a target for stepped $\chi_{e,HP}$ recognition (shot #22507). Top to bottom: ECRH power; electron temperature from ECE; central line density; major radius. Central temperature drops according to the density increase.

wave propagation performed at current flat-top. The feedback loop for radial position control is less effective at low currents, and the plasma centre oscillates by a few mm during EC power modulation, which requires particular care in analysing ECE data and reconstructing heat wave propagation.

As shown in figure 12, both the experimental amplitude and the phase reveal a sudden drop in diffusivity at $r = 0.075$–0.095 m, well away from the EC deposition layer. The low and high diffusivities on the two sides of the transition layer are different by an order of magnitude, and the jump is localized in a narrow layer. Figure 13 shows where the transition in the diffusivity is located with respect to the $1/L_T$ profile and the q-profile, the gradient length L_T coming from the ECE $T_e(r)$

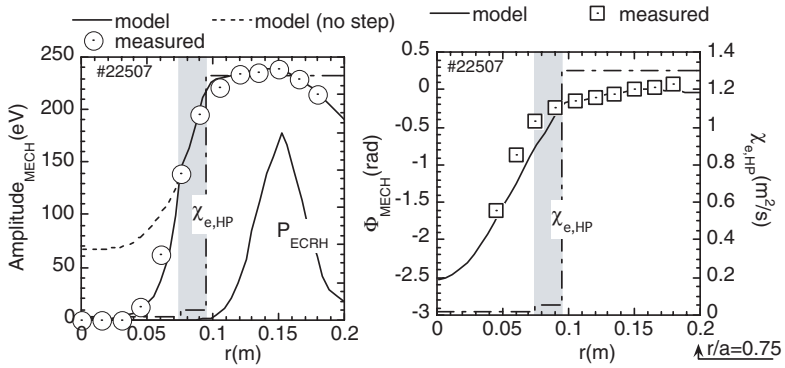

Figure 12. This figure shows the amplitude (left) and phase distribution of an inward heat wave launched at $r = 0.15$ m by modulated EC power, in a low current discharge without sawteeth, with $q_0 > 1$. The heat wave detects, unambiguously both in amplitude and phase, a large step-down in $\chi_{e.HP}$ in the narrow layer $r = 0.075$–0.095 m.

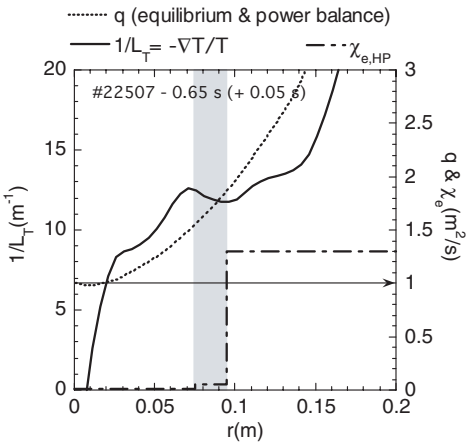

Figure 13. The position of the high–low diffusivity transition is compared in the figure with the q profile provided by equilibrium reconstruction and power balance, and with the radial distribution of the inverse temperature gradient length. As in most cases observed in FTU, the step in $\chi_{e,HP}$ is positioned at the radius where $1/L_T$ stops increasing with increasing radius, and tends to clamp to its saturation value because of stiffness. In contrast, the transition does not appear to occur at rational values of the safety factor q.

measurements and the safety factor q being estimated from equilibrium reconstruction with power balance constraints.

The analysis of these shots, confirming a common feature found in all MECH experiments performed on FTU with off-axis absorption and inward heat wave propagation, leads to the important result that the step in $\chi_{e,HP}$ is intrinsic to the plasma self-organization, in the sense that it is not always strictly localized at the EC heating position. If the heat flux from EC wave absorption is largely dominant, as observed in most ECRH experiments so far (e.g. [12]), the step in $\chi_{e,HP}$ is located at the absorption layer. Instead, while confirming that with strong EC heating the step is located at the absorption layer, we show that at reduced P_{ECRH} the transition survives but at a point different from absorption and closer to the axis.

As demonstrated in shot #22507, the step position is not related to the $q = 1$ surface, which is absent in this case. Also the location of low-order rational surfaces does not appear to be well correlated with the transition in diffusivity.

Possibly, the transition is located at the inner margin of the region where L_T is saturated, which is fully consistent with predictions of the critical gradient model for electron energy transport, and with the implications of equation (1).

5. Detection of EC absorption radius for real-time control applications

The results of electron transport studies with ECRH show the existence of a transition layer in thermal diffusivity, that isolates a central region with good confinement, and supporting the idea that the transition is localized when the T_e gradient exceeds a critical limit. However, the question of what really controls the value of the critical gradient length and the position of the transition layer is still open. To perform experimental research and quantitative studies on the relationship between heat flux, temperature gradient and criticality, ECRH experiments with precise control of heat flux distribution would be most useful.

However, in order to take a step further and obtain total control of all the details of the experimental configuration, some degree of feedback action is required for controlling the EC beam. It is well-known, for example, that the Shafranov shift will change the effective absorption radius due to the change of stored energy during ECRH, which in turn could depend on the absorption radius itself. This non-linear response could cause inefficient use of experiments programmed with purely feed-forward procedures, in the sense that the effective deposition radius could turn out to be quite different from what is expected, and therefore feedback action is strongly recommended. To implement reliable feedback on the absorption radius (e.g. on the beam steering angle) the automatic recognition of the real EC absorption radius is necessary in real-time.

In addition to heat transport studies, localized ECRH/ECCD is a promising tool for a variety of applications, such as TM stabilization, sawtooth-crash triggering (or suppression), internal transport barrier control and detection and formation of advanced scenarios. In all cases the knowledge of the real absorption radius is important for the understanding of experimental results. In some cases, as for NTM stabilization or sawtooth control, the intervention of ECRH/ECCD shall eventually be automatic and in real-time in fusion reactors,

requiring continuous information on the absorption radius for a correct feedback action. In case several EC beams are to be used contemporarily, possibly each one heating a different layer, real-time detection of all absorption radii is indeed a difficult task.

Well-known techniques for reconstruction of the power deposition profile $P_{EC}(r)$ are based on a fast change of the EC power and a fast measurement of the electron temperature profile (e.g. [20]). ECE diagnostic is preferable, because of the close relation between emission and absorption, and the frequency instead of the radius can be used as the ordering parameter. Two complementary techniques are feasible: Switching on or off the ECRH with monitoring of the T_e ramp-rate radial profile (e.g. [21–23]), or modulated ECRH with monitoring of the fluctuating amplitude distribution (e.g. [24]). In both cases, in order to provide an accurate $P_{EC}(r)$ profile the timescale for T_e measurement has to be fast, in principle much shorter than the heat diffusion time across the absorption layer δ_{dep}. Since, in most cases, the typical order of magnitude of the absorption layer width is $\delta_{dep} \approx 0.03$ m, and the thermal diffusivity is of the order of $\chi_e \approx 1\ m^2\ s^{-1}$, it follows that the characteristic diffusion time $\tau_{diff} = \delta^2/\chi_e$ is of the order of a ms, and modulation frequencies in the kHz range, or above, are needed.

The MECH technique can, in principle, provide continuous monitoring of r_{dep}, but at the expense of a non-negligible fraction of the total power available for the specific ECRH application. Depending on the amplitude modulation width, the resulting average power is always less than the maximum power continuously deliverable by the gyrotrons.

The on/off method is available for free at the beginning and at the end of the ECRH pulse, but in order to provide information within the heating period, the pulse on/off has to be repeated. This can be achieved by switching off gyrotrons, for a short time (≈1 ms), with a repetition rate determined by a trade-off between time resolution and power lost for heating during off time.

The two methods are discussed in what follows, paying particular attention to the reliability in the localization of the absorption peak, rather than to the accurate description of the whole deposition profile.

6. High modulation frequency

The r.f. output of gyrotrons can in principle be modulated at very high frequencies, as for all electronic tubes, by pulsing either the main h.v. power supply for diode-type tubes, or the cavity power supply for depressed collector gyrotrons. In both cases, the real limitation in frequency comes from the power supply itself, and more precisely from the bandwidth imposed by the feedback loop of the main regulated high voltage power supply and from the output current capability of the cavity power supply.

In the ECRH system on the FTU tokamak, a series tetrode fine regulating unit and a hex-phase bridge rectifier, thyristor-controlled power supply provides regulated beam voltage at 70 kV [25]. With this system 0–100% output power modulation can be obtained at a frequency up to 10 kHz, with a negligible harmonic distortion content on the beam voltage and a slightly distorted waveform on the output power. The actual voltage waveform can be composed of up to five components with different frequencies and amplitudes.

High modulation frequency in adiabatic conditions means, in general, low amplitude of electron temperature oscillations δT_e, since $nk\delta T_e \approx P_{EC} t_{mod}/2$, t_{mod} being the modulation period. It follows that deep modulation (≈100%) is needed at high frequency, with a reduction of average absorbed power with respect to the maximum deliverable by the gyrotrons. In case of experiments dedicated to heating power distribution reconstruction this drawback is acceptable, and the results can be compared with theoretical estimates based on ray tracing or, better, beam tracing calculations [26]. Figure 14 shows the experimental distribution of T_e oscillations at the modulation frequency of 5 kHz in the case of a moderately off-axis absorption on the FTU tokamak at relatively low density ($n_{e,line} \approx 0.4 \times 10^{20}\ m^{-3}$). Experimental data are compared with beam tracing calculations, showing good agreement if the finite spatial resolution of the ECE diagnostic is taken into account. The centre of experimental data (12 fast ECE channels are available on the FTU tokamak) coincides with the calculated absorption peak position within a distance less than half the radial channel separation (≈12 mm in this case). In case more gyrotrons are used, they could be distinguished by using different modulation frequencies.

The method can be applied also in the presence of TMs at approximately the same frequency, the two contributions to the oscillating T_e being separable unless they are exactly at the same frequency. Figure 15 shows the ability of the analysis of MECH data at high modulation frequency to discriminate true modulation from MHD effects. Fast Fourier analysis can distinguish the two contributions, provided that the frequencies are separated by some amount. Since the

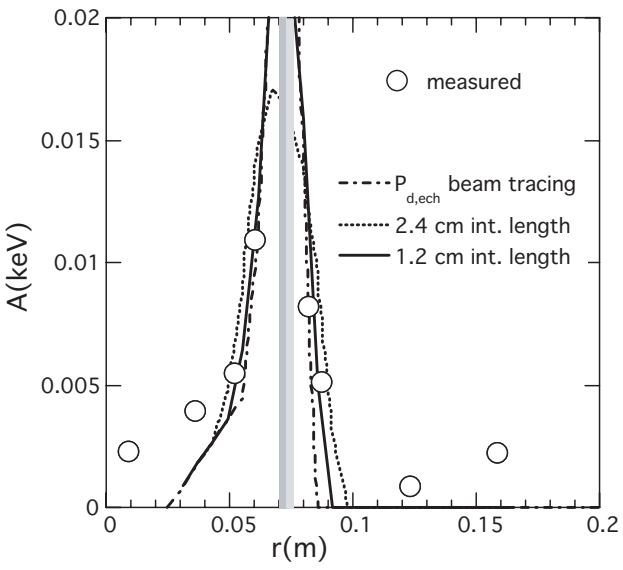

Figure 14. The figure shows a comparison between the EC absorbed power density profile, calculated by a beam-tracing code, and the measured amplitude distribution of the electron temperature oscillations at the modulation frequency of 5 kHz, which is about five times higher than the inverse diffusion time $1/\tau$ across the calculated absorption layer width. The experimental data fit well with the calculated profile, once it is integrated over the scale length corresponding to the spatial resolution of the ECE diagnostic, and appropriately scaled in amplitude.

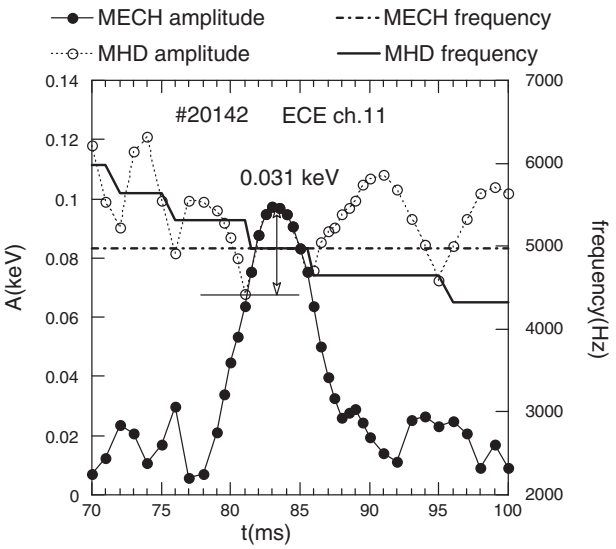

Figure 15. The figure shows the ability of the analysis of MECH data at high modulation frequency to discriminate true modulation from MHD effects. Closed circles correspond to the peak amplitude in the FFT spectrum at the modulation frequency, while open circles correspond to the MHD component. When the two frequencies are close, beating between MHD and MECH components appears.

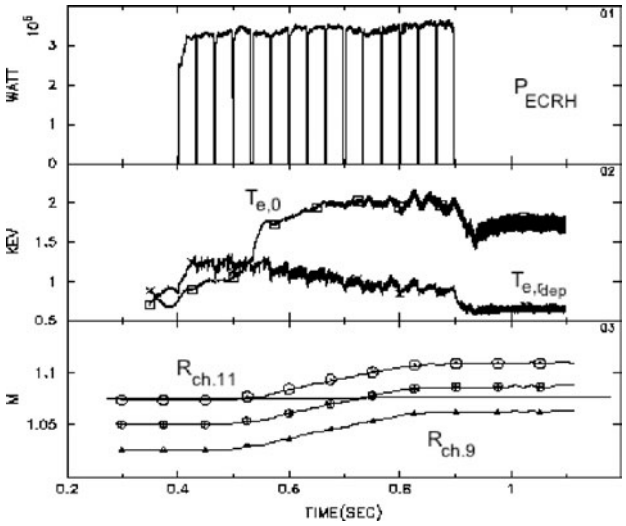

Figure 16. The figure shows the main features of the RPO technique for real-time recognition of the EC absorption radius. Top to bottom: ECRH power; electron temperature at centre and at the absorption radius; the major radii of the three ECE channels closest to EC resonance. EC absorption occurs at $r/a \approx 0.4$ (horizontal line, bottom figure). The EC power is repetitively switched off for a very short time interval (3 ms in this case), while keeping the power on with a high duty cycle.

frequency of MHD oscillations usually varies in time, exact frequency overlapping occurs only for very brief periods. In the case, shown in the figure, when the two frequencies are very similar but not equal (at $t = 83 \pm 2$ ms), the beating amplitude can be used to reconstruct the different contributions of the two oscillations (MECH and MHD). For these conditions $A_{\mathrm{MHD}} + A_{\mathrm{MECH}} = A_{\mathrm{Max}}$ and $A_{\mathrm{MHD}} - A_{\mathrm{MECH}} = A_{\mathrm{min}}$, A_{Max} and A_{min} being, respectively, the maximum and minimum of the beating amplitude.

7. Repetitive pulse on/off

The main drawback of high frequency MECH for on-line r_{dep} recognition is that, in order to be applicable, deep modulation is necessary, leaving unused a substantial fraction of the gyrotron power. In addition, real-time data analysis is quite cumbersome, Fast Fourier transformation being necessarily required.

An alternative method is described here, consisting of the repetitive switching off of the gyrotron for a short time (1–3 ms) and with a repetition rate low enough to provide almost full available average power. The repetitive pulse off (RPO) technique is an application of the traditional on/off methods mentioned earlier, with a less stringent requirement of r_{dep} localization capability only, and not of full power deposition profile reconstruction. On the other hand, the use of the simplest numerical analysis, compatible with implementation in fast real-time digital signal processors is an important additional requirement for real-time applications. The main aim of the experiments performed was, therefore, to verify that this simplified data analysis has the capability of tracking a moving EC absorption position in a plasma affected by thermal and positional instabilities.

A typical discharge used for testing the RPO method is shown in figure 16. Strong MHD activity affects the whole plasma column, creating fast oscillations in the temperature measurements in all channels of the ECE diagnostic system used for this application. The electron temperature profile switches from hollow to peaked at $t \approx 0.54$ s, as shown by the time evolution at the centre and at $r/a = 0.4$. The presence of temperature instabilities on different timescales allows verification of the reliability of the method.

In order to check the capability of the RPO technique to identify r_{dep} and to follow in real-time a drifting absorbing layer, a small ramp on the toroidal field was applied. This causes a corresponding drift of the radial (major radius) position of all the measuring ECE channels. At the same time, off-axis deposition was achieved by steering the EC beam from shot to shot in such a way as to absorb the wave almost at the same flux surface during the B_{tor} ramp (figure 17). During the ramp, therefore, the absorption peak shifts through ECE channels.

Since all the details of the switch-off method are well-described in the literature, we focus here mainly on the data analysis used in the RPO application. Basically, a linear fit of the electron temperature varying in time is performed on a time base τ_{lin}, which is longer than the period of MHD instabilities, τ_{MHD}, and shorter than the energy confinement time, τ_E. In the experiments performed τ_{lin} was set to 1 ms. The linear fit is made before (left time derivative $(\mathrm{d}T_{\mathrm{e}}/\mathrm{d}t)^-$) and after (right time derivative $(\mathrm{d}T_{\mathrm{e}}/\mathrm{d}t)^+$) each on–off transition (the EC power is switched in less than 50 μs). The change in slope, multiplied by the local electron density, is a measure of the local heating power density. A significant improvement in the signal-to-noise ratio is achieved by adding the contribution of more pulses, using boxcar integration. The absorption radius r_{dep} is localized at the position of the ECE channel where the change in slope is the largest.

The result of the analysis of the case in figure 16 is shown in figures 18 and 19. In figure 18 the distribution between the

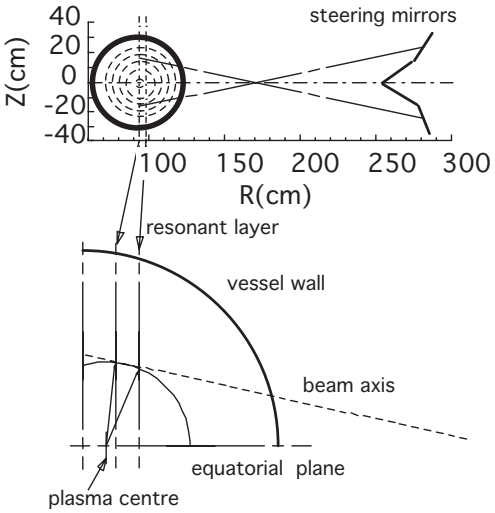

Figure 17. The scheme of the relative position of EC beams axis and plasma column is shown in the figure. With this arrangement, although a toroidal field scan moves the resonant layer and the ECE grid of measuring points along the minor radius, the EC absorption remains peaked on the same magnetic surface. Therefore, the ECE grid moves with respect to the ECH absorption.

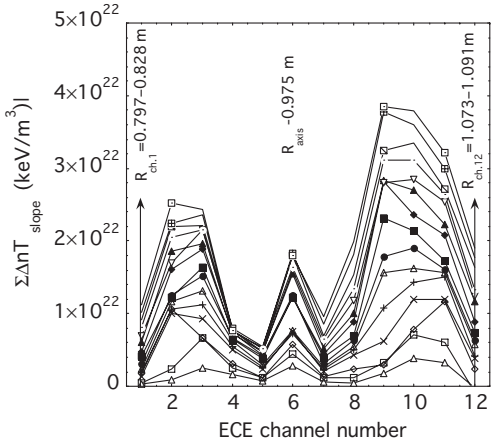

Figure 18. Cumulative jump of the rate of change in the local stored electron energy in each channel of the ECE polychromator at switching on of the ECRH power. The nT quantity at each pulse is added up in order to increase the signal to noise ratio, simulating a box-car integration technique. The measuring grid displacement during the $B_{\rm tor}$ ramp is shown by the motion of the peak in $\sum \Delta nT$ from ≈channel 11 at earlier times (on the low field side) to ≈channel 9 later on.

ECE channels of the change in pressure slope is shown, the different lines being obtained by adding pulses one after the other. In figure 19 the channel with maximum increase is shown versus pulse number (in practice, versus time). Absorption is localized between channels 10 and 11 at the beginning of the $B_{\rm tor}$ ramp, and between channels 9 and 10, as expected, at the end.

In case $B_{\rm tor}$ is kept constant, the system detects no change in the channel with highest $\delta(n\,{\rm d}T/{\rm d}t)$. In case of on-axis heating, when both absorption and channel positions are expected to change during $B_{\rm tor}$ ramp by the same amount, the maximum of $\delta(n\,{\rm d}T/{\rm d}t)$ occurs at the same ECE polychromator channel.

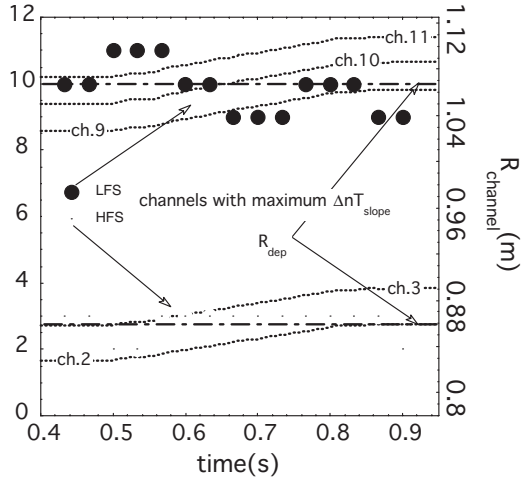

Figure 19. For a better description of the response of the RPO technique to movements of the measuring grid with respect to the EC absorption radial profile during $B_{\rm tor}$ ramp, both the radii of the channels nearest to absorption, and the position of the ECE channels detecting the largest jump in the rate of change in the stored energy, are shown in the figure. As $B_{\rm tor}$ is increased, and the radii of ECE channels of the low field side are also increased, the maximum $\Delta({\rm d}nT/{\rm d}t)$ moves accordingly from channels 10 and 11 to channels 9 and 10. In the high field side the radii move to a much less extent, and so does the channel number with maximum $\Delta({\rm d}nT/{\rm d}t)$. This shows that the RPO technique is sensitive to movements of the EC absorption radius of the order of an ECE channel separation.

The RPO technique is, therefore, able to track the absorption radius dynamics, and it can be used as the basis of real-time control applications.

8. Conclusions

Experiments on electron transport with ECRH, steady state and transient, both during flat-top and during current ramp-up, support the description of the plasma having a well-confined core, separated from a region of enhanced transport. Regions of enhanced transport are also characterized by temperature profile stiffness. The transition layer is an intrinsic plasma feature, appearing at the radius where the gradient length $L_{\rm T}$ saturates, possibly approaching a critical value $L_{\rm T,c}$. In the presence of strong and localized ECRH, the transition in the electron thermal diffusivity is located at the absorption layer. These results are all in agreement with the modelling of electron transport, and of the electron temperature profile stiffness, based on the critical gradient length assumption.

Concerning the possible use of ECRH in real-time control applications, the RPO technique has the potential for reliable automatic detection of the EC deposition radius. When compared to high frequency MECH, the RPO method does not waste significant EC power. In addition, RPO data analysis can be performed by algorithms suitable for implementation in fast digital signal processors.

References

[1] Hoshino K. *et al* 1995 *Proc. 15th Int. Conf. on Plasma Physics and Controlled Nuclear Fusion Research (Seville, 1994)* vol 1 (Vienna: IAEA) p 697

[2] Cirant S. *et al* 2000 *Proc. 18th Int. Conf. on Fusion Energy 2000 (Sorrento, 2000)* CD-ROM file EX3/3 and http://www.iaea.org/programmes/ripc/physics/fec2000/html/node1.htm
[3] Gantenbein G. *et al* 2000 *Phys. Rev. Lett.* **85** 1242
[4] Pietrzyk Z.A. *et al* 1999 *Nucl. Fusion* **39** 587
[5] Cirant S. *et al* 2001 *Fusion Eng. Des.* **53** 301
[6] Cirant S. *et al* 1999 *Proc. 13th Conf. on Radio Frequency Power in Plasmas, AIP Conf. Proc.* **485** 221
[7] La Haye R.J. *et al* 2002 *Phys. Plasmas* **9** 2051
[8] Fujita T. *et al* 2002 *Fusion Energy 2002* CD-ROM file OV/1-3 and http://www.iaea.org/programmes/ripc/physics/fec2002/html/fec2002.htm
[9] Sozzi C. *et al* 2000 *Fusion Energy 2000* CD-ROM file EXP5/13 and http://www.iaea.org/programmes/ripc/physics/fec2000/html/node1.htm
[10] Cirant S. *et al* 2001 *14th Conf. on Radio Frequency Power in Plasmas, AIP Conf. Proc.* **595** 338
[11] Ryter F. *et al* 2000 *Fusion Energy 2000* CD-ROM EX2/2 and http://www.iaea.org/programmes/ripc/physics/fec2000/html/node1.htm
[12] Ryter F. *et al* 2001 *Phys. Rev. Lett.* **86** 2325
[13] Minardi E. and Weisen H. 2001 *Nucl. Fusion* **41** 113
[14] Sozzi C. *et al* 2002 *Proc. 29th Conf. on Plasma Phys. and Controlled Fusion* vol 26B (ECA) P-1.048
[15] Jacchia A. *et al* 2001 *14th Conf. on Radio Frequency Power in Plasmas, AIP Conf. Proc.* **595** 342
[16] Ryter F. *et al* 2002 *Proc. 29th Conf. on Plasma Phys. and Controlled Fusion* vol 26B (ECA) P-1.048
[17] Jacchia A. *et al* 2002 *Nucl. Fusion* **42** 1116
[18] Bruschi A. *et al* 2001 *Fusion Eng. Des.* **53** 431
[19] Cirant S. *et al* 2001 *Fusion Eng. Des.* **53** 301
[20] Erckmann V. and Gasparino U. 1994 *Plasma Phys. Control. Fusion* **36** 1869
[21] Cirant S. *et al* 1995 *11th Conf. R.F. Power in Plasmas, AIP Conf. Proc.* **355** 159
[22] Leuterer F. *et al* 1997 *24th EPS Conf. Proc.* vol 21A, p 1533
[23] Andreev V.F. *et al* 1999 *26th EPS Conf. on Controlled Fusion and Plasma Physics (Maastricht, 14–18 June 1999)* vol 23J (ECA) pp 853–6
[24] Romè M. *et al* 1997 *Plasma Phys. Control. Fusion* **39** 117
[25] Sozzi C. *et al* 1999 *14th Topical Conf. on R.F. Power in Plasmas, AIP Conf. Proc.* **485** 462
[26] Nowak S. *et al* 2002 *Proc. 12th Workshop on ECE and ECRH (Aix-en-Provence, 13–16 May 2002)*